Effects of Chirality at Tyr13 on the Structure−Activity Relationships of ω-Conotoxins from *Conus magus*†

Katherine J. Nielsen, Denise A. Adams, Paul F. Alewood, Richard J. Lewis, Linda Thomas, Tina Schroeder, and David J. Craik*

Centre for Drug Design and Development, The University of Queensland, Brisbane, 4072

Received December 18, 1998; Revised Manuscript Received February 16, 1999

ABSTRACT: The effects of chirality inversions of Tyr13 on the structure−activity relationships of ω-conotoxins MVIIA and MVIIC were examined using a combination of 2D ^{1}H NMR spectroscopy and radioligand binding studies specific for N-type ([^{125}I]GVIA) and P/Q-type ([^{125}I]MVIIC) voltage-sensitive calcium channels (VSCCs). A comparison of the Hα secondary shifts suggests that the structural scaffolds of MVIIA and MVIIC are little altered by the L- to D- inversion of Tyr13; however, the conformations of several residues in loop 2 (residues 9−14) are significantly altered. The experimentally determined 3D structure of [D-Y13]MVIIA indicates that the positions of key residues in this loop which are involved in the binding of MVIIA to the N-type VSCC (Tyr13, Arg10, and Leu11) are so changed as to render the peptide unrecognizable by its cognate ion channel. The large reduction in potency observed for MVIIA and MVIIC at both N-type and P/Q-type VSCCs is likely to stem from the change in conformation and orientation of loop 2.

The ω-conotoxins from piscivorous cone snails target a number of different voltage-sensitive calcium channels (VSCCs)[1] in vertebrates, including the N-type VSCC which is widely distributed throughout the central and peripheral nervous system, and the P/Q-type VSCC which is found primarily at the neuromuscular junction channel. They act by selectively preventing Ca^{2+} entry into the nerve terminal during a presynaptic action potential, thereby inhibiting transmitter release (*1*). The ω-conotoxins are basic peptides of 24−29 residues that have an amidated C-terminus and include six cysteine residues which form three disulfide bridges, arranged to give a characteristic 4-loop framework (Figure 1). All of the ω-conotoxins adopt a consensus tertiary structure (*2*) despite considerable differences in noncysteine primary sequence (*3*).

Since the ω-conotoxins display a range of selectivities for different subtypes of the neuronal VSCCs, they make excellent tools for studying and treating certain neuropathologies such as head trauma and pain (*4*). Of particular interest is ω-conotoxin MVIIA (Figure 1), which selectively blocks N-type VSCCs and is currently in phase III of human clinical trials for intractable pain (*5*). However, MVIIA has side effects which include hypotension and shaking (*6, 7*). Knowledge of how MVIIA binds to the N-type VSCC may be useful in developing improved therapies and possibly small molecule mimetics of ω-conotoxins useful in pain relief.

There have been several studies aimed at determining which residues on MVIIA, and its relative GVIA, are responsible for binding to the N-type VSCC (*8*−*16*). Early studies led to the proposal of the two-point binding region involving Lys2 and Tyr13 of GVIA and MVIIA. Later studies have shown that additional residues may also be involved in binding, including Arg21, Arg10, and Leu11 of MVIIA (*14*), and in addition, Arg17, Tyr22, and Lys24 of GVIA (*15*). However, it is apparent in all studies that Tyr13 makes the greatest contribution to binding to the N-type VSCC and thus can be considered the primary binding determinant. Less is known about ω-conotoxin interactions with P/Q-type VSCCs; however, Tyr13 is also conserved in MVIIC which binds to the P/Q-type VSCC subtype preferentially.

To investigate the influence of Tyr13 orientation on ω-conotoxin binding, we replaced it with its D analogue in both MVIIA and MVIIC, and examined the structure−activity relationships (SARs) developed from radioligand assays that measure potency of binding to N-type and the P/Q-type VSCCs. [D-Y^{13}]MVIIA and [D-Y^{13}]MVIIC were examined using ^{1}H NMR spectroscopy, and their secondary Hα shifts compared with those of the parent peptides to determine whether structural changes result from the chiral inversions. To investigate the extent of these structural changes, the 3D structure of [D-Y^{13}]MVIIA was determined and compared to that of MVIIA.

† This work was supported by a GIRD grant from the Department of Industry, Science and Technology, and AMRAD Corporation Ltd.

* To whom correspondence should be addressed. Australian Research Council Professorial Fellow. Phone: 61-7-3365-4945. Fax: 61-7-3365-2487.

[1] Abbreviations: VSCC, voltage-sensitive calcium channel; NMR, nuclear magnetic resonance; 2D, two-dimensional; 3D three-dimensional; DQF-COSY, double quantum filtered-correlated spectroscopy; NOESY, nuclear Overhauser enhancement spectroscopy; TOCSY, total correlated spectroscopy; E-COSY, exclusive correlated spectroscopy; RMSD, root means square deviation; MVIIA, ω-conotoxin from Conus magus; MVIIC, ω-conotoxin from Conus magus; Boc, *tert*-butoxycarbonyl; ESMS, electrospray ionisation mass spectrometry; RP-HPLC, reversed-phase high-performance liquid chromatography; LC/MS, HPLC, combined with mass spectrometry; Pam, phenylacetylamidomethyl; *p*-MBHA, *p*-methylbenzhydrylamine; RLB, radioligand binding studies.

10.1021/bi982980u CCC: $18.00
Published on Web 05/05/1999

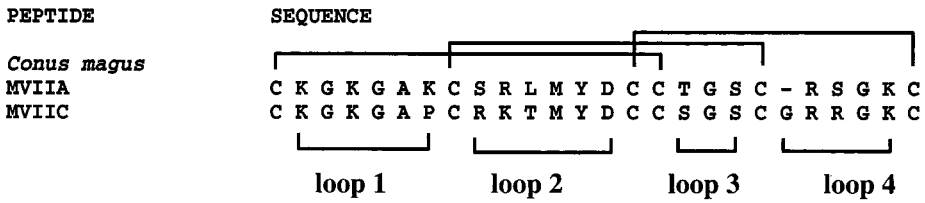

FIGURE 1: The sequence of ω-conotoxins MVIIA and MVIIC showing the positions of the disulfide bridges and the 4-loop structure.

In general, understanding the effects of L−D inversion on peptide SARs is important since increasing examples of the posttranslational modification of specific amino acids [e.g., Ser46 in ω-agatoxin-TK (*17*) and Trp4 in D-contryphan (*18*)] are being found in nature. Such inversions may occur for a number of possible reasons including improved potency, increased protection from degradation enzymes, and structural change. Inversion of configuration is also of great interest in peptide synthesis, not only for traditional applications of protection from enzymatic degradation but more recently for modulating folding properties. For example, synthetic [D-Ala^5]GVIA, where a glycine residue was replaced, was able to fold to the correct disulfide bonded isomer and 3D structure, whereas the L analogue could not be folded (*15*). In this study, we successfully synthesized D-Y^{13} analogues of MVIIA and MVIIC and determined their SARs.

EXPERIMENTAL PROCEDURES

Peptide Synthesis. Materials. Synthesis of C-terminal amidated peptides was conducted on *p*-MBHA resin, obtained from Peptide Institute. The substitution value was 0.79 mequiv/g. Boc protected amino acids were obtained from Peptide Institute. The side-chain protection chosen for the Boc amino acids was Arg(Tos), Asp(OcHxl), Lys(ClZ), Thr(Bzl), Tyr(BrZ), Ser(Bzl), and Cys(*p*-MeBzl). All other Boc amino acids used were side chain unprotected. DMF, DCM, DIEA, and TFA were all of peptide synthesis grade from Auspep (Melbourne, Australia). 2-(1-Hydroxy-1,2,3-benzotriazol-1-yl)-1,1,3,3-tetramethyluronium hexafluorophosphate (HBTU) was obtained from Quantum Biotechnologies (France). Acetonitrile and methanol (Hipersolve-Far UV grade) were from BDH (Poole, U.K.). Water was obtained from a tandem Millipore Milli-RO−Milli-Q system. *p*-Cresol and *p*-thiocresol were from Fluka (Germany). HF was supplied by BOC Gases (Brisbane, Australia). Ammonium acetate (AR) and ammonium sulfate (AR) were from AJAX Chemicals (Australia). Guanidine·HCl (99%+) and reduced and oxidized glutathione were from Sigma Aldrich.

A Waters 600 HPLC system equipped with an autoinjector was used for all RP-HPLC. The buffer systems used for all analysis were A (0.1% TFA in H_2O) and B (0.09% TFA, 10% H_2O, and 90% CH_3CN). Analytical RP-HPLC was conducted on a Vydac C18, 5 μm (0.46 × 25 cm) column. Samples were run using a 1% gradient (100% A, 5 min; 100% A to 60% B, 60 min) at 1 mL/min and monitored at 214 nm; final purity was also confirmed on a 1% gradient at 280 nm. A Vydac C18, 5 μm (1.0 × 25 cm) column was used for semipreparative RP-HPLC with a flow rate of 3 mL/min, and a Vydac C18, 10 μm (2.2 × 25 cm) column was used for preparative RP-HPLC with a flow rate of 8 mL/min.

Mass spectra were measured on a PE Sciex API-III triple quadrupole ion spray mass spectrometer. Amino acid analysis was performed on all the synthetic peptides. This involved hydrolyzing the samples in vacuo for 24 h at 105 °C with 6 M HCl. Samples were then derivatized with phenyl isothiocyanate (*19*) and analyzed by HPLC using the Waters Picotag method (Waters Operator's Manual no. 88140).

Peptide Synthesis. Peptides were assembled by manual stepwise synthesis on *p*-MeBHA resin (0.5 mmol scale) using BOC chemistry methodology (*20*). Removal of the Boc protecting group prior to coupling was accomplished by shaking in 100% TFA for 2 × 1 min. DMF was used for flow washes and as the coupling solvent. Each amino acid (2 mmol) was double coupled when ninhydrin values indicated less than 99% coupling. If coupling remained less than 99%, the remaining amino groups were acetylated using acetic anhydride in DMF (87 μL/mL).

After assembly, the peptides were released from the resin using HF. The *N*-α-Boc group was first removed (TFA, 2 × 1 min) and the peptide was washed with DCM and dried under nitrogen. Cleavage from the resin and simultaneous deprotection of side chains was carried out in liquefied HF in the presence of the scavengers *p*-cresol and *p*-thiocresol (18:1:1 by volume) at −5 to 5 °C for 1.5 h. HF was removed under vacuum, and the peptide was precipitated with cold, oxygen-free ether, collected by filtration on a sintered funnel, and washed with cold, oxygen-free ether to remove scavenger adducts. The peptide was dissolved in 45% aqueous acetonitrile, further diluted with water, and lyophilized.

The crude reduced peptides were purified by preparative chromatography, using a 1% gradient (100% A to 80% B, 80 min) with a flow rate of 8 mL/min and UV detection at 230 nm. Fractions were collected and analyzed by electrospray mass spectrometry. Fractions which gave the desired mass were then analyzed by analytical RP-HPLC to confirm purity, and those fractions which were pure were combined and lyophilized to give the reduced peptide.

Purified reduced peptides were oxidized at a concentration of 0.02 mM in either aqueous 0.33 M NH_4OAc/0.5 M GnHCl ([D-Y^{13}]MVIIA), or aqueous 2 M $(NH_4)_2SO_4$/0.1 M NH_4-OAc ([D-Y^{13}]MVIIC) with pH adjusted to 7.5−8.0 using 0.01 M NH_4OH. The solution was stirred for 3−5 days at 4 °C, in the presence of reduced and oxidized glutathione (molar ratio of peptide:GSH:GSSG was 1:100:10). The reaction mixtures were sampled periodically and analyzed by RP-HPLC, and eluant fractions were collected for electrospray mass spectrometric analysis. When LC and MS analysis confirmed that oxidation was complete, the oxidation was terminated by lowering the pH to 2−3 with TFA.

Oxidized peptides were purified by loading the acidified reaction mixtures onto a preparative column at a flow rate of 8 mL/min, washing with 100% A until all oxidation buffer had eluted, and then applying a 1% gradient (100% A to

80% B, 80 min) with a flow rate of 8 mL/min and UV detection at 230 nm. Fractions were collected and analyzed as for the reduced peptides. If further purification was necessary, the peptide was repurified on a semipreprative column on a 1% gradient (100% A to 80% B, 80 min) with a flow rate of 3 mL/min and UV detection at 230 nm. Fractions were collected and analyzed as before.

Preparation of [^{125}I]GVIA and [^{125}I]MVIIC. Peptides were iodinated using (1,3,4,6-tetrachloro-2a,6a-diphenyl-glycuoluril) (IODO-GEN) (*21*−*23*). A total of 10 μL of the peptide, 5 μL (5.75 mg/mL, 17.4 mCi/mg) of Na^{125}I (DuPont NEN, New research products, Boston), and 25 μL of sodium phosphate buffer (50 mM, pH 7.4) were added to an eppendorf tube coated with IODO-GEN (Pierce, Rockford) and incubated for 5 min. The reaction mixture was vortexed and then equilibrated for 5 min prior to purification.

Preparative HPLC of ^{125}I-labeled peptides was performed on a Waters 680 gradient controller equipped with two Waters 510 HPLC pumps and a Waters 481 absorbance detector. Peptides were analyzed on a VYDAC reversed-phase C-18 analytical column (4.6 × 250 mm) eluted at 1 mL/min with a linear gradient of 0 to 67% of solvent B over 100 min: solvent A, 1% TFA (trifluoroacetic acid); solvent B, 90% CH_3CN + 0.09% TFA. Separation was monitored at 214 nm, and 1 mL fractions were collected. Fractions of interest were detected with a LKB Wallac 1272 automatic γ counter.

To confirm the identity of iodinated peptides, mass spectrometry was performed. HPLC fractions from peptides iodinated with nonradioactive K^{127}I were injected directly into the mass spectrometer. Mass spectra were acquired on a Apple Macintosh IIfx computer using the software package MacSpec (Sciex, Toronto).

Radioligand Binding Studies. Crude rat membrane was prepared as described in ref *24*. Briefly, rats were sacrificed by cervical dislocation, their brains were rapidly removed and dissected on ice. The remaining steps were performed at 4 °C. Tissue was homogenized in 50 mM HEPES, pH 7.4, with a Polytron (at half-speed) and the homogenate centrifuged for 15 min at 40000*g*. The pellet was resuspended in 50 mM HEPES, pH 7.4, and 10 mM EDTA and incubated for 30 min on ice. It was then recentrifuged at 40000*g* for 10 min and the pellet resuspended in 50 mM HEPES, pH 7.4, using the Polytron. Protein concentration was estimated using a BCA protein assay reagent (Pierce, Rockford).

Ligand binding assays were run in triplicate in glass tubes at room temperature (*14*, *25*). Each tube contained between 250 and 600 nM of the nonlabeled peptide (except for [D-Y^{13}]-MVIIA and [D-Y^{13}]MVIIC, where concentrations up to 10 μM were used), 5−10 fmol of the radiolabeled peptide, and 16 μg of crude rat membrane in a total volume of 300 μL. Filters (Whatman GF/B 25 mm glass fiber filters) were soaked in 0.6% polyethyleneimine for 1 h to reduce nonspecific binding. Incubation was terminated by washing the tubes with 3 × 3 mL of ice-cold wash buffer (20 mM HEPES, 125 mM NaCl, and 0.1% BSA, pH 7.2) and filtering under vacuum. The radioactivity bound to the filters was counted with a LKB Wallac 1272 automatic γ counter. Filter blanks were determined by filtering 50−100 pM of the radiolabeled peptide. The data were analyzed using GraphPad Prism 2.0 (GraphPad Software, Inc, San Diego, USA).

^{1}H NMR Spectroscopy. NMR spectra were recorded on Bruker ARX 500 or DMX 750 spectrometers equipped with a *z*-gradient unit. Peptide concentrations were 2 mM (pH 3.5) in 95% H_2O/5% D_2O and 100% D_2O. ^{1}H NMR experiments run were DQF-COSY (*26*), E-COSY (*27*), NOESY (*28*, *29*) with mixing times of 400, 200, and 120 ms and TOCSY (*30*) with a mixing time of 120 ms. All spectra were recorded at 293 K with additional NOESY spectra recorded at 280 K.

Spectra were recorded over 6024 Hz with 4096 data points, 512−600 FIDs, 16−64 scans and a recycle delay of 1.0 s or 1.5 s for DQF-COSY and E-COSY. In NOESY and TOCSY experiments, the solvent was suppressed using the WATERGATE sequence (*31*). Spectra were processed using UXNMR. FIDS were multiplied by a polynomial function and apodized using a 60 or 90° shifted sine-bell function in both dimensions prior to Fourier transformation. Baseline correction using a fifth order polynomial was applied, and chemical shifts were referenced externally to DSS at 0.00 ppm. $^3J_{NH-H\alpha}$ coupling constants were measured from high resolution 1D spectra (32 K) and compared to those obtained from a DQF-COSY spectrum transformed at high digital resolution (8192 × 1024) and extracted using the Lorentzian line-fitting routine in the program Aurelia (Bruker GMBH). $^3J_{H\alpha-H\beta}$ coupling constants were measured directly from E-COSY spectra transformed to high digital resolution (8192 × 1024) over the region of interest.

Distance Restraints and Structure Calculations. Peak volumes in 120 ms NOESY spectra (in H_2O and in D_2O) were classified as strong, medium, or weak corresponding to upper bounds on interproton distances of 2.7, 3.5, or 5.0 Å, respectively. The 120, 200, and 400 ms NOESY spectra were monitored to ensure that no spin diffusion artifacts were incorporated into restraints. Peaks that were observed only in the long mixing time (400 ms) NOESY spectrum were classified as very weak and the corresponding distances were assigned an upper bound of 6.0 Å. In all cases, lower distance bounds were set to 1.8 Å. Appropriate pseudo-atoms were made (*32*), and a distance of 0.5 Å was added to the upper limits of restraints involving methyl protons. $^3J_{NH-H\alpha}$ coupling constants were used to determine ϕ dihedral angle restraints (*33*) and $^3J_{H\alpha-H\beta}$ coupling constants together with relevant NOESY peak strengths were used to determine χ_1 dihedral angle restraints (*34*). Where there was no diastereospecific assignment for a prochiral pair of protons, the larger upper bound for the two restraints was used but where stereospecific assignments were established, the distances were specified explicitly.

Structures were calculated using the simulated annealing protocol in X-PLOR (*35*, *36*), version 3.1, using the geometric force field, parallhdg.pro. Starting structures were generated using random (ϕ,ψ) dihedral angles and energy minimized (500 steps) to produce structures with correct local geometry. The structures were subjected to a total of 30 ps of high-temperature molecular dynamics before cooling to 0 K and final energy minimization (1000 steps). Structure refinements were performed using energy minimization (2000 steps) under the influence of the CHARMM force field (*37*).

Table 1: pIC_{50} Values, 95% Confidence Intervals (CI) and Change in Potencies (ΔP) for MVIIA, MVIIC, and Their D-Y^{13} Analogues

peptide	pIC_{50} (CI) [^{125}I]MVIIC	pIC_{50} (CI) [^{125}I]MVIIC	ΔP^a	ΔP^b
MVIIA	10.87 (10.83−10.91)	7.14 (7.06−7.22)	0	2.3
[D-Y^{13}]MVIIA	7.24 (7.19−7.28)	<5	3.6	>4.4
MVIIC	8.23 (8.19−8.28)	9.39 (9.36−9.43)	2.6	0
[D-Y^{13}]MVIIC	6.08 (5.85−6.31)	5.61 (5.45−5.79)	4.8	3.8

[a] Change in potency calculated from the difference in pIC_{50} values of the peptide from the pIC_{50} values of MVIIA. [b] Change in potency calculated from the difference in pIC_{50} values of the peptide from the pIC_{50} values of MVIIC.

Data Analysis. Structures were compared using pairwise and average RMSD values for the Cα, C, and N atoms (X-PLOR, version 3.1) and by calculating angular order parameters for the backbone dihedral angles (*38*, *39*). Structure visualization and superimpositions were done using InsightII 95 (Biosym Technology, Inc., San Diego).

RESULTS

Peptide Synthesis. MVIIA, MVIIC, and their D-Y^{13} analogues were synthesized in high yield using solid-phase peptide synthesis as described in the Experimental Procedures. The purified reduced peptides were oxidized in the presence of reduced and oxidized glutathione to produce the correctly folded product.

Radioligand Binding Assays. The binding affinity of MVIIA, MVIIC, and their D-Y^{13} analogues to the N-type and P/Q-type VSCCS were measured from the ability of these ligands to displace [^{125}I]GVIA and [^{125}I]MVIIC, respectively from VSCCs in rat brain membrane. The IC_{50} values together with 95% confidence intervals and relative potencies, determined by nonlinear curve fitting algorithms, are given in Table 1. The D analogues of MVIIA and MVIIC both exhibited significant reductions in potency compared to their L counterparts. Data from [^{125}I]GVIA and [^{125}I]-MVIIC binding assays were complementary with respect to the relative change in potencies (ΔP). For example, the analogue [D-Y^{13}]MVIIA has a ΔP toward the N-type VSCC of 3.6, while its MVIIC counterpart has a ΔP toward the P/Q-type VSCC of 3.8. Similarly, [D-Y^{13}]MVIIA was inactive against [^{125}I]MVIIC having a ΔP of 4.8, which is mirrored by [D-Y^{13}]MVIIC having a ΔP of at least 4.4 at the P/Q-type VSCC. These results support previous work that suggests that Tyr13 is crucial for high affinity VSCC binding in rat brain (*10*−*12*, *14*). They also indicate that Tyr13 is as important for the potency of MVIIC toward P/Q-type VSCCs as it is for MVIIA binding to N-type VSCCs. The higher potency of MVIIA toward the N-type VSCC compared to MVIIC at the P/Q-type VSCC is therefore likely to be due to the presence of additional binding interactions in MVIIA.

^{1}H NMR Spectroscopy. Spectral Assignment. ^{1}H NMR spectra were recorded at 500 and 750 MHz for [D-Y^{13}]-MVIIA and [D-Y^{13}]MVIIC, and these were assigned using the sequential assignment protocol (*40*). Ambiguities in the assignments due to peak overlap were resolved by comparison of NOESY and TOCSY spectra recorded at different temperatures. An illustration of the spectral quality and generally good NH dispersion is given in Figure 2A, which shows a TOCSY spectrum of [D-Y^{13}]MVIIA with spin system assignments for selected residues. For [D-Y^{13}]MVIIA and [D-Y^{13}]MVIIC, all residues have narrow line widths, except for those in loop 2 (residues 9−14) where the signals are weak due to line-broadening. This provides an indication that loop 2 of these peptides undergoes conformational exchange. The fingerprint region of the NOESY spectrum shown in Figure 2B further highlights the good spectral dispersion of NH and Hα protons and documents the sequential resonance assignments from Cys16 to Cys25. The complete chemical shift assignments for [D-Y^{13}]MVIIA are provided in the Supporting Information.

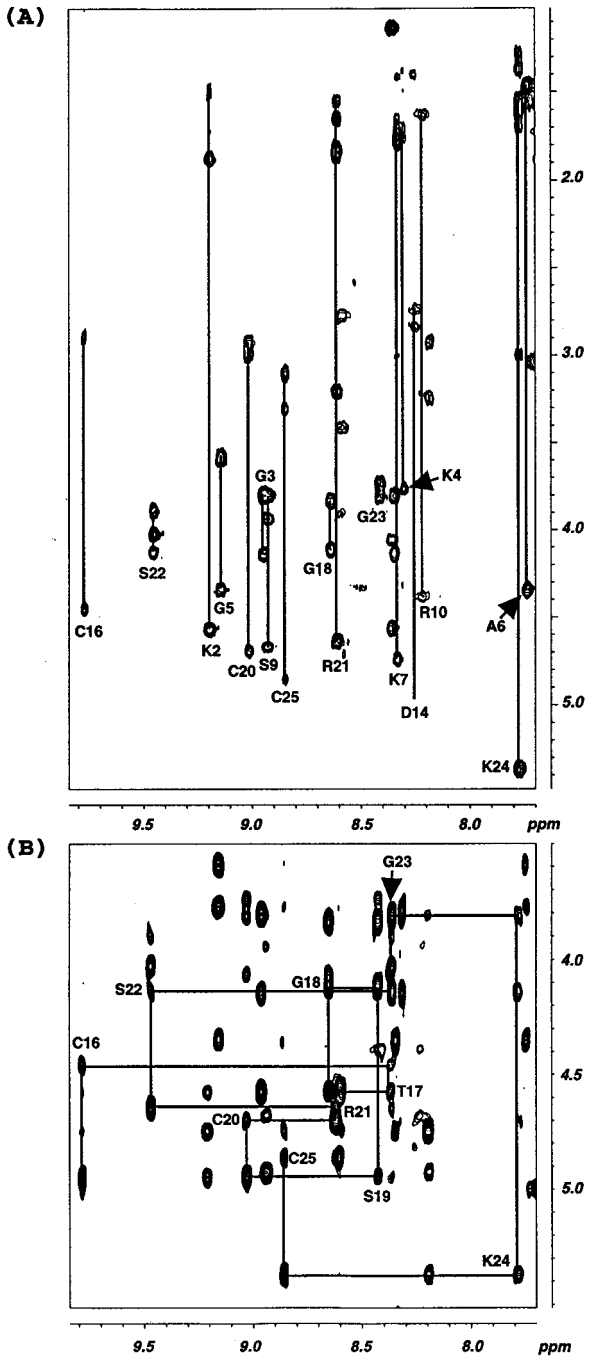

FIGURE 2: ^{1}H NMR spectra of [D-Y^{13}]MVIIA. (A) The NH-side-chain region of the TOCSY spectrum (750 MHz, 293 K, pH 3.5) detailing spin systems of K2−C15; and (B) NH−Hα region of the NOESY spectrum (750 MHz, 293 K, pH 3.5) showing the sequential assignment of C16−C25.

Hα Chemical Shifts. The secondary shifts, i.e., chemical shifts relative to random coil values (*41*), of the Hα protons are a sensitive measure of backbone conformation (*42*, *43*). In this study, secondary Hα shifts were used in the first instance to check that the global fold of the native peptides was maintained in the two analogues and to monitor changes in local structure that may have resulted from mutation. Figure 3A shows that the pattern of Hα secondary shifts is almost identical for all four peptides, reflecting that each adopts a similar global fold. However, there are a number of differences at individual residues (Figure 3B), primarily those located in loop 2, suggesting that the chirality inversion of Tyr13 affects the structure of the MVIIA and MVIIC mutants in this region. Ser19 is the only residue outside loop 2 where there is a significant difference in secondary shift. The chemical shift changes are observed for both mutant peptides, indicating that the same set of conformational changes occur upon the chirality inversion of Tyr13 in MVIIA and MVIIC (Figure 3B).

Judging by the secondary Hα shifts in MVIIA, these conformational changes involve Arg10 and Leu11 in addition to Tyr13, all of which are considered important for binding to the N-type VSCC. Despite having apparently little effect on the ω-conotoxin global fold, the point mutation of Tyr13 may have deleterious effects on the structure of loop 2 and, hence, the binding of the peptide to the N-type VSCC. This loop is implicated in VSCC affinity and specificity (*14*), and therefore, it is important to determine the nature of these structural changes and their ramifications in VSCC binding. To address the influence of structure on activity, we determined the solution structure of [D-Y^{13}]MVIIA (see below). Since the secondary Hα shifts indicate that the structural differences between [D-Y^{13}]MVIIA and [D-Y^{13}]-MVIIC, and their parent peptides were identical, 3D structural calculations were not obtained for [D-Y^{13}]MVIIC.

2D TOCSY and NOESY spectra were recorded for MVIIA and [D-Y^{13}]MVIIA at two pH values (3.5 and 6.0) to evaluate whether their structures were altered by changes in pH. A comparison of the effects of pH on the Hα chemical shifts is given in Figure 3C. The results show that there is no detectable conformational difference in the backbone of MVIIA or [D-Y^{13}]MVIIA at these two pH values. The only significant difference in Hα chemical shift (>0.05 ppm) is for Cys1, which is likely to be due to the effects of differing charge states at the N-terminus rather than a conformational change. Even the NH shifts (Figure 3D), which in other peptides are generally more susceptible to environmental changes, show little alteration in chemical shift over this pH range. Only the NH proton of Ser9 in MVIIA exhibited a significant ($\sim$0.1 ppm) chemical shift significant dependence on pH, while the same residue in [D-Y^{13}]MVIIA has an NH proton shift of 0.34 ppm over this pH range. In addition, the NH proton of Lys2 in [D-Y^{13}]MVIIA changes by 0.1 ppm, consistent with the charge difference at the N-terminus at the different pH values. They are not likely to be due to differences in conformation, since these changes are not mirrored by Hα chemical shifts.

These results indicate that the structures of MVIIA and [D-Y^{13}]MVIIA are similar at pH 3.5 to those at more physiologically relevant pH values and further reinforce the notion that the structure of the ω-conotoxins is conserved in a variety of solution environments (*2*). Not unexpectedly, some protons have increased exchange with H_2O at the higher pH (i.e., the NH protons of Ser22, Met12, and Arg10 are not visible at pH >6.0), and therefore, the structure of [D-Y^{13}]MVIIA was based on ^{1}H NMR data recorded on the sample at pH 3.5 where all resonances were observable.

Secondary Structure of [D-Y13]MVIIA. The most significant long-range NOEs observed in [D-Y^{13}]MVIIA are summarized in Figure 4. As in the native peptide (*2*, *44*, *45*), the dominant element of secondary structure for [D-Y^{13}]MVIIA is a triple-stranded β-sheet. In both peptides, residues 19−20 form a peripheral β-strand, linked to the central β-strand (residues 24−25) by a β-turn. The other peripheral β-strand is formed by residues 6−8. One long-range NOE found in MVIIA is missing in [D-Y^{13}]MVIIA (20 Hα−25 Hα); however, this is most likely due to peak overlap as all the remaining NOEs which define the β-sheet region are present. In addition to the triple-stranded β-sheet, two short antiparallel strands comprising residues 1−2 and 14−16 form a β-bridge in [D-Y^{13}]MVIIA. While this has not been reported explicitly in previous studies of MVIIA (*2*, *44*−*45*), the characteristic NOEs are indeed observed in MVIIA (unpublished results), confirming the presence of this element of secondary structure in the native peptide. In support of this the β-bridge structure has been reported for κ-conotoxin PVIIA which has the same disulfide connectivities and similar 3D structure to the ω-conotoxins (*46*).

The major differences between MVIIA and [D-Y^{13}]MVIIA are demonstrated by differences in the local and medium-range NMR data. A summary of the sequential backbone NOEs for [D-Y^{13}]MVIIA is given in Figure 5, together with $^3J_{NH-H\alpha}$ coupling constants, slow-exchange NHs, and medium range NOEs. For residues 1−8 and 15−25, the NMR data are almost identical to those described previously for MVIIA (*2*), supporting the notion that these peptides adopt a similar structure. However, there are significant differences over loop 2 where several medium-range NOEs observed for MVIIA are absent in the mutant peptide. In MVIIA, these NOEs define a series of overlapping turns (*2*) but in [D-Y^{13}]-MVIIA, these turns are evidently altered. This is supported by the observation of broadened lines for the amide protons in this region, which precluded measurement of $^3J_{NH-H\alpha}$ coupling constants, and is also reflected by differences in the secondary Hα shifts in this region (Figure 3A).

The NMR data also suggest unexpected changes in the orientation of loop 2. For example, a set of key long-range NOEs between the Hα protons of residue 10 and the Hβ protons of Cys20 in MVIIA and MVIIC is replaced by NOEs between the Hα protons of residue 11 and the Hβ protons of Cys20 in the two mutants studied here. These NOEs are indicative of the proximity of loops 2 and 4 and may explain the Hα secondary shift changes observed for Ser19 in [D-Y^{13}]-MVIIA and [D-Y^{13}]MVIIC.

3D Structure of [D-Y13]MVIIA. A set of 50 structures of [D-Y^{13}]MVIIA was calculated using a simulated annealing protocol based on 246 NOE-derived distance restraints (114 intraresidual, 62 sequential, and 62 long-range) and 18 distance restraints defining 9 H-bonds, 16 ψ dihedral restraints, and 7 χ_1 side chains dihedral restraints. The 16 lowest energy structures were chosen to represent [D-Y^{13}]-MVIIA and are shown superimposed in Figure 6A. The molecule is well-defined over most residues but is clearly

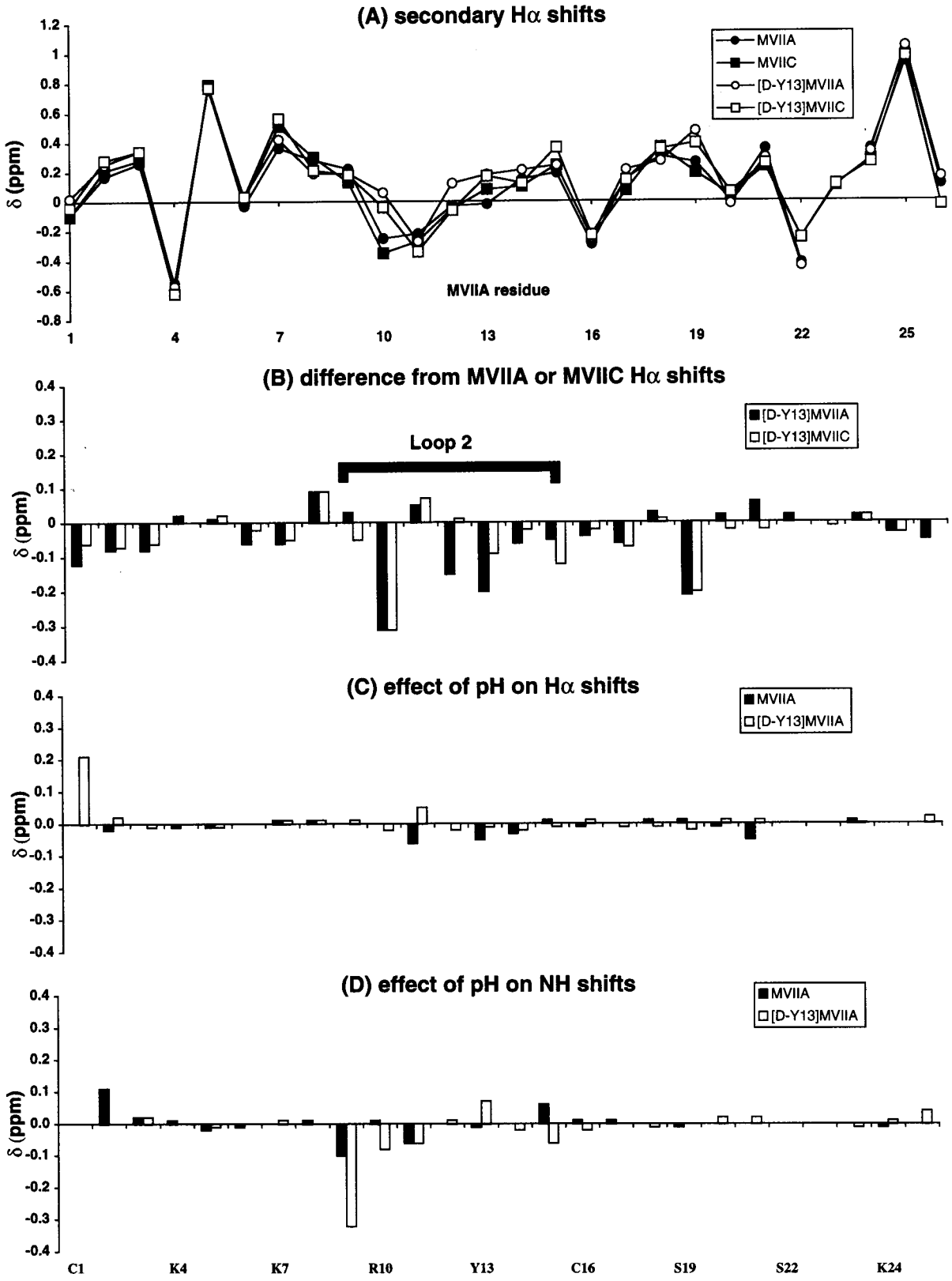

FIGURE 3: (A) Secondary Hα shifts for native MVIIA (filled circle), MVIIC (filled square), [D-Y^{13}]MVIIA (empty circle) and [D-Y^{13}]-MVIIC (empty square) showing the similarity in global fold and (B) differences in chemical shift between MVIIA and [D-Y^{13}]MVIIA (filled column) and between MVIIC and [D-Y^{13}]MVIIA (unfilled column), which emphasize the structural difference between the mutant and native peptides in loop 2 (Ser9 to Asp14) and at Ser19. The effects of pH on the (C) Hα and (D) NH chemical shifts are given for MVIIA (filled columns) and [D-Y^{13}]MVIIA (empty columns).

less structured in loop 2. The pairwise root-mean-square deviation (RMSDs) for the set of structures is 0.44 Å for the backbone atoms and 1.81 Å for all heavy atoms. The corresponding values for residues excluding loop 2 (i.e., residues 1−8 and 16−25) are 0.36 and 1.40 Å, respectively. The angular order parameters (S) for the ϕ and ψ backbone dihedral angles, together with RMSDs among the set of structures for each residue, are given in Figure 7. The higher

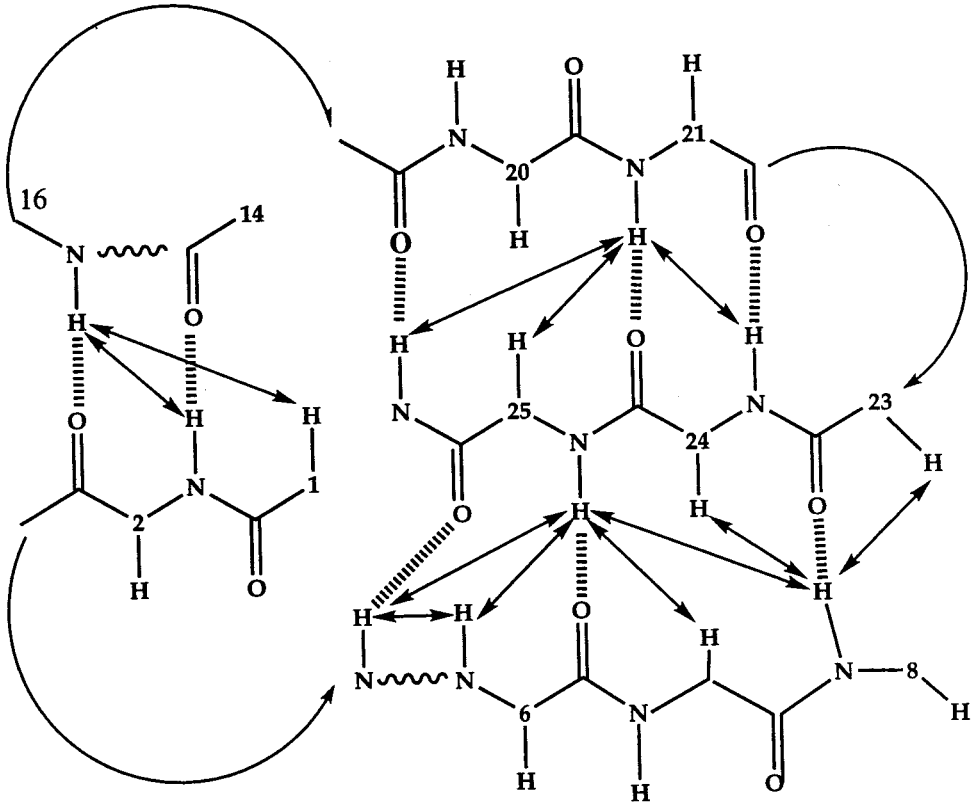

FIGURE 4: Representation of the secondary structure dominated by the triple-stranded β-sheet and β-bridge in [D-Y[13]]MVIIA. Double-stranded arrows indicate observed NOEs, dashed lines represent putative hydrogen bonds and curved single-headed arrows represent β-turns.

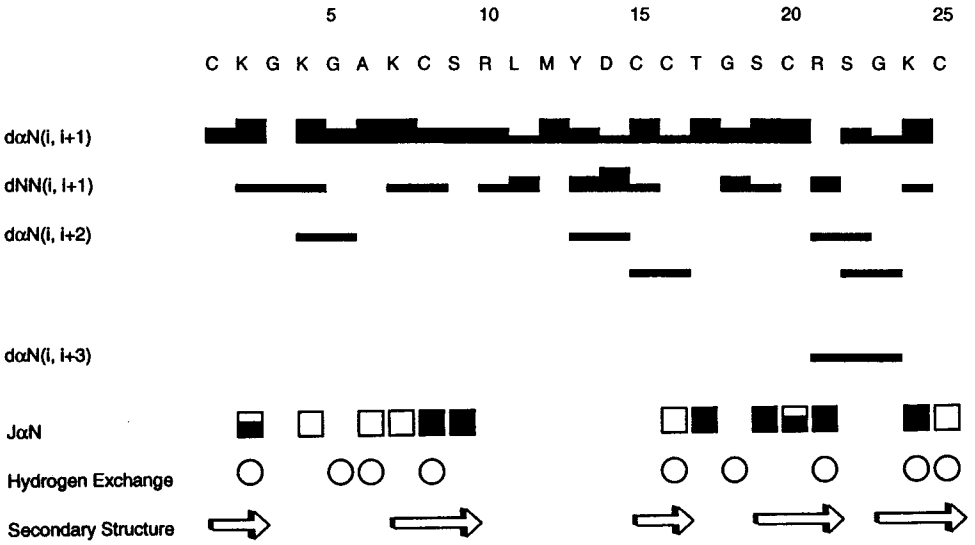

FIGURE 5: Summary of local and medium range NMR data for [D-Y[13]]MVIIA. The height of the bars indicate the strength of the NOE; Filled, 2/3 filled and unfilled squares represent $^3J_{NH-H\alpha}$ coupling constants of >9 Hz, 8−9 Hz and <6 Hz, respectively. Open circles indicate slow exchange NH protons (>30 min). The β-sheet and β-bridge regions are denoted by arrows at the bottom of the diagram.

RMSD values seen in loop 2 (residues Arg10 to Asp14) most likely reflect the fewer NOEs observed compared to the remainder of the molecule. The angular order parameters for the backbone dihedral angles $S(\phi)$ and $S(\psi)$ also differ in loop 2. Over most of the molecule, $S(\phi)$ and $S(\psi)$ values are close to unity (average ≥ 0.97), except for Leu11 and Met12 where they are low (<0.6), again indicating that the structure of this peptide is poorly defined in loop 2. Thus, the 3D structure of [D-Y[13]]MVIIA identifies the same regions of disorder that were independently indicated by the Hα secondary shift changes.

Comparative views of MVIIA and [D-Y[13]]MVIIA (Figure 6) indicate that these structures are similar overall, but different in loop 2. In MVIIA, loop 2 is almost "U-shaped", and residues Ser9−Tyr13 are exposed and oriented away from loop 4. However, in [D-Y[13]]MVIIA, loop 2 is flattened by comparison and oriented toward loop 4. In addition, the positions of the side chains of Ser9−Tyr13 are altered relative to their positions in MVIIA. While the side chain of Tyr13 is clearly affected by the change in chirality, other residues also have significantly altered positions, most notably Arg10 and Leu11. This is important as these residues

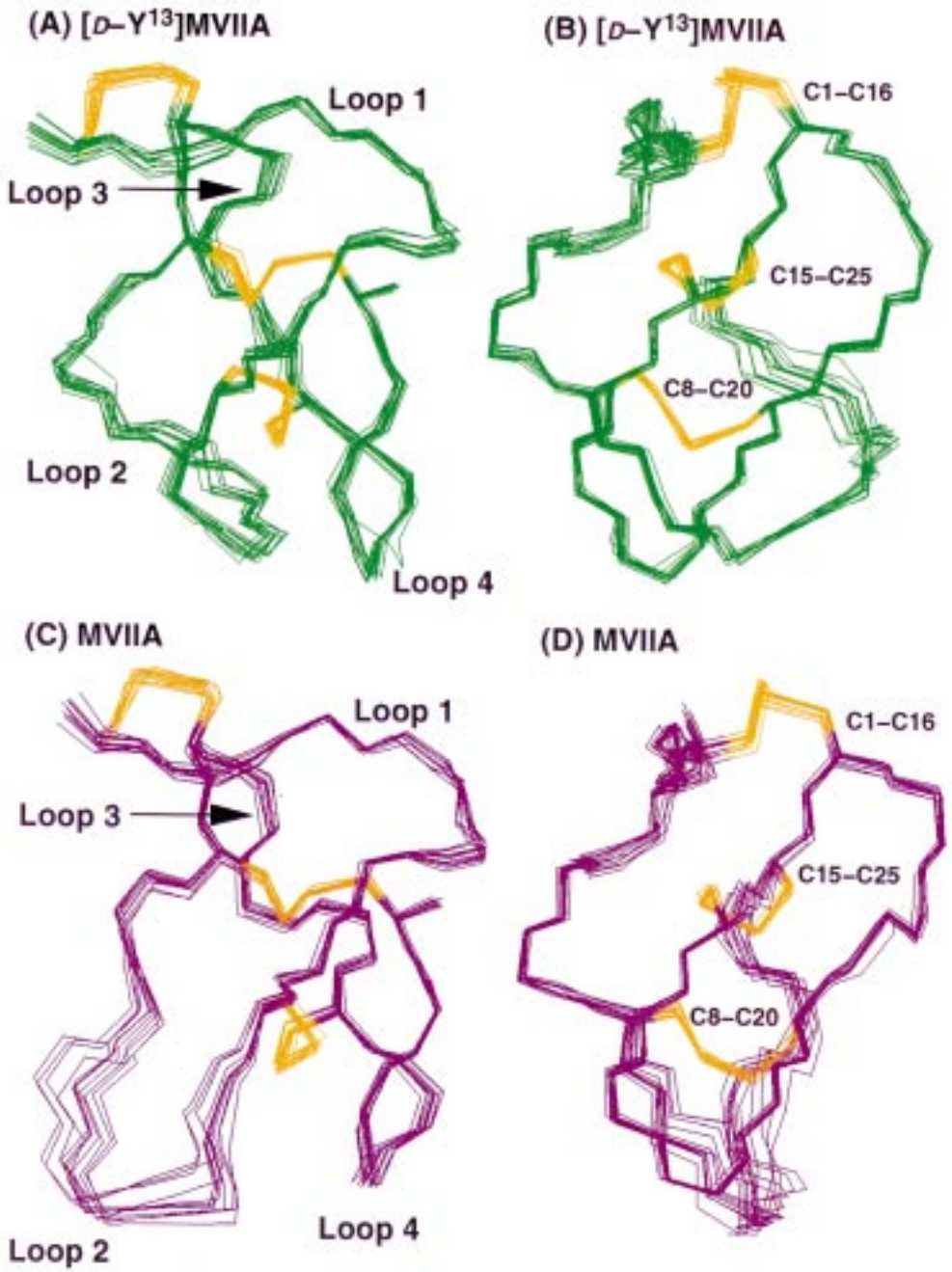

FIGURE 6: (A) A global backbone superimposition of the 16 lowest energy structures of [D-Y^{13}]MVIIA showing the backbone atoms (green) and the disulfide bridges (orange). The positions of the loops are also indicated. The structures were superimposed over the backbone atoms of residue 1−9 and 14−25, with an average RMSD of 0.36 Å. (B) shows the same structures rotated in a 90_{-y}°. The structures in panels A and B are compared with those of MVIIA (backbone purple; from ref *2*) in the same relative orientations in panels C and D, respectively.

have been shown to have a significant impact on MVIIA binding to VSCCs (*14*). The relative positions of these two residues and Tyr13 in MVIIA and [D-Y^{13}]MVIIA are shown in Figure 8.

A measure of the extent of change in the positions of the side chains of Tyr13, Arg10, and Leu11 is obtained by comparing distances between a reference heavy atom on each side chain under consideration (i.e., CZ in Arg10, CG in Leu11 and CZ in Tyr13) and between the same atoms and the center of mass (denoted as pseudoatom X). It is of interest to note that the center of mass of each structure was relatively invariant within and between the sets of structures. The atoms pairs in [D-Y^{13}]MVIIA and MVIIA for which distances were compared are shown schematically in Figure 8, detailing clearly two triangular pyramids of different dimensions and orientations. These measurements are summarized in Table 2, together with the average improper angle θ, defined by atoms X−Y13(CZ)−L11(CG)−R10(CZ). With respect to the center of mass, the X−R10 distances are not changed significantly, whereas X−Y13 and X−L11 distances are reversed in [D-Y^{13}]MVIIA and MVIIA. The improper angle, θ, outlined in Figure 8 shows clearly that the locations of the atoms at the verteces of these pyramids are different, with Tyr13 and Leu11 essentially swapping positions in MVIIA and [D-Y^{13}]MVIIA. Thus, the comparison of the 3D structures of MVIIA and [D-Y^{13}]MVIIA indicates that the

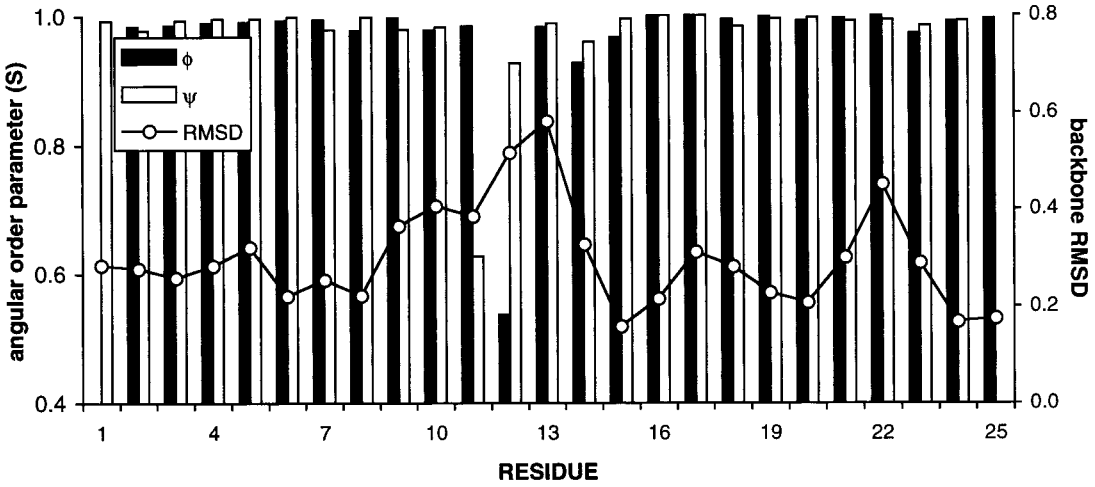

FIGURE 7: RMSD values (Å) and the angular order parameters (*S*) for the ϕ and ψ backbone dihedral angles of [D-Y^{13}]MVIIA versus residue number.

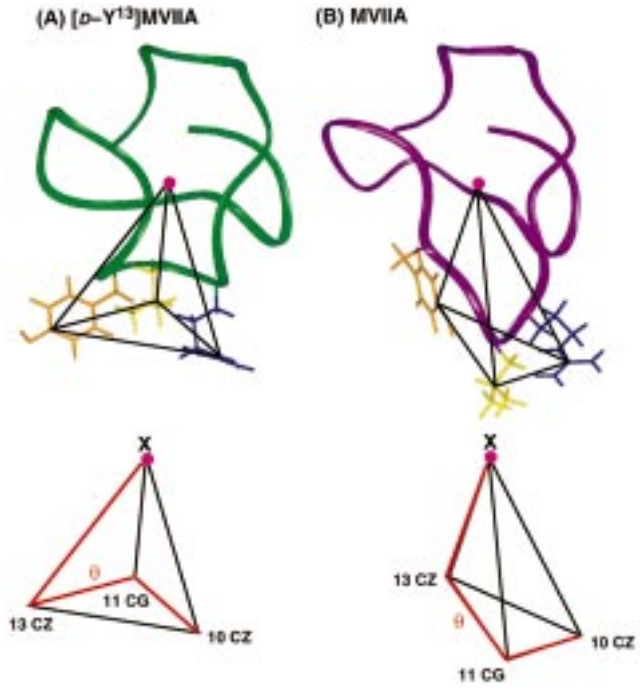

FIGURE 8: A representative structure of [D-Y^{13}]MVIIA (green) and MVIIA (purple) showing the triangular pyramid formed by the atoms CZ in Arg10 (blue), CG in Leu11 (yellow), CZ in Tyr13 (orange) and the pseudoatom defining the center of mass (pink). The black lines join the atom pairs for which distances were measured. Below, the triangular pyramids are shown with the improper angle (θ) outlined in red.

positions of these three residues, all of which are important for the high potency of MVIIA, are affected by the chirality inversion of Tyr13.

The results show that the effects of a change in chirality at Tyr13 are not just localized to this residue, but also involve other residues in loop 2, although the global fold is clearly maintained. It is informative to compare the degree of surface exposure for residues that have altered positions compared to MVIIA (Figure 9). Aside from Tyr13, the surface profiles of [D-Y^{13}]MVIIA and MVIIA are almost identical, despite the fact that the conformations of loop 2 residues are significantly affected by the chirality inversion of Tyr13. It thus appears that the L−D inversion causes a redistribution in the 3D placement of residues in loop 2, but does not alter the total surface exposure of the relative exposure of individual side chains.

Table 2: Average Distances (Å) between Atom Pairs and Average Value of the Improper Angle (X−Y13-L11-R10) Calculated for the Set of MVIIA and [D-Y^{13}]MVIIA Structures

distance (Å)	MVIIA	[D-Y^{13}]MVIIA
Y13 (CZ)−L11 (CG)	7.7 ± 0.8	10.0 ± 1.4
L11 (CG)−R10 (CZ)	8.2 ± 2.0	6.7 ± 1.6
R10 (CZ)−Y13 (CZ)	8.2 ± 1.8	11.2 ± 3.2
X[a]−R10 (CZ)	11.5± 1.3	10.5 ± 0.9
X−L11(CG)	11.0 ± 0.9	8.0 ± 0.4
X−Y13 (CZ)	7.9 ± 0.7	10.8 ± 0.7
	Improper Angle (deg)	
X−Y13−L11−R10	−92.9 ± 16.6	94.6 ± 15.2

[a] X is a pseudoatom representing the center of mass of each structure.

DISCUSSION

It has previously been proposed that the region Cys8−Cys15 is the most flexible part of the ω-conotoxin structure and more sensitive to substitution than other regions because of a lack of stabilizing interactions (*15*). It is in this region that Tyr13 is positioned and the orientation of this residue is likely to be important for VSCC affinity since it has been shown to be the primary binding determinant of ω-conotoxins/VSCC interactions in rat brain (*11*, *12*, *14*, *15*). From radioligand binding studies and functional assays, it may be estimated that the Tyr−Ala replacement of residue 13 in GVIA contributes to a ~500-fold reduction in potency (*15*). This result has led to the suggestion that the reduction in binding reflects the removal of a direct binding interaction of Tyr13 with the VSCC, rather than simply a secondary conformational change since the conformational effects of this substitution appear to be negligible in the unbound ligand, at least in the case of GVIA (*15*). Replacement of Tyr13 with a phenylalanine in MVIIA causes a ~300-fold reduction in binding (*14*, *16*), indicating that the hydroxyl-moiety of the tyrosine is a key factor in VSCC binding.

In the current study, we have investigated the influence that the orientation of Tyr13 has on binding through an analysis of D-Y^{13} analogues. The L−D substitution of Tyr13 in MVIIA reduces the potency for the N-type VSCC in rat

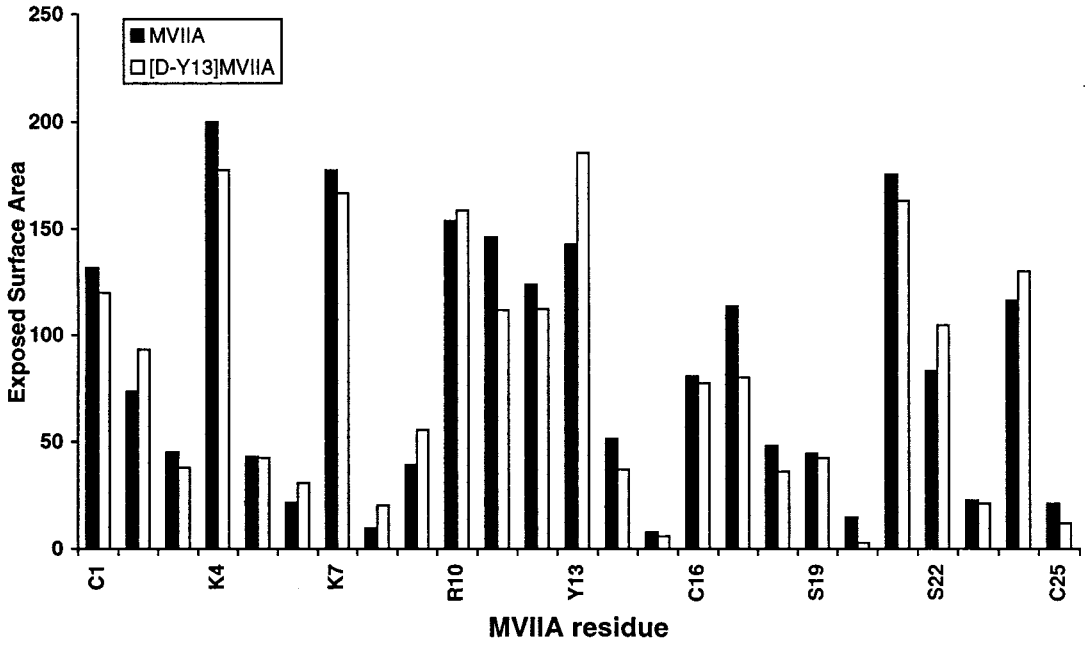

FIGURE 9: The surface profile of MVIIA and [D-Y^{13}]MVIIA showing the surface exposed area (Å^2) for each residue, calculated using a 1.4 Å radius probe.

brain by ~4000-fold. This reduction in potency is greater than what may be expected from previous studies on Tyr13 mutants. The results from this study show this cannot be attributed solely to a chirality inversion of Tyr13 and that additional structural changes are involved. These include local conformational changes that are likely to prevent several binding interactions with the VSCC. The presence of D-Tyr13 alters the orientation of loop 2, altering the positions of several key residues on the surface of the molecule in addition to Tyr13, thereby affecting its ability to recognize the ω-conotoxin binding site on the ion channel.

The change in conformation associated with [D-Y^{13}]MVIIA is greater than might be expected from a point mutation. The conformation and orientation of loop 2 is evidently finely balanced, with the whole of this region susceptible to structural change. In contrast, the rest of the backbone that forms the structural scaffold retains its structural integrity, being almost identical to the native peptide, MVIIA. Importantly, replacement of the Tyr13 with the D analogue significantly changes the orientation of the side chains of Leu11 and Tyr13, and to a lesser extent, Arg10. Since Arg10 and Leu11 contribute significantly to the potency of MVIIA at N-type VSCCs, changes in the positions of these residues must also be considered in the analysis of the binding data. Therefore, we propose that the reduction in binding affinity of [D-Y^{13}]MVIIA to the N-type VSCC stems from the loss of (i) a possible hydrogen-bond from the hydroxyl group of Tyr13 (*11*), (ii) a hydrophobic interaction from Leu11, and perhaps also (iii) a putative electrostatic interaction from Arg10 (*14*). Although Met12 also alters its position, it is not likely that this influences binding, since this residue plays a minimal role in binding as assessed by mutation studies (*14*), despite being relatively exposed.

In this study, the conformational effects of the Tyr13 substitution appear to be identical for MVIIA and MVIIC. However, the reductions in potency observed for the D analogues are less for the P/Q-type VSCC than for the N-type VSCC, suggesting that Tyr13 is either less important or that a different set of interactions occur in P/Q-type VSCC binding. One possibility is that fewer residues in loop 2 of MVIIC interact with the P/Q-type VSCC compared to MVIIA/N-type VSCC interactions and therefore disruptions in loop 2 have less effect. This is supported by the observation that MVIIC is less potent toward the P/Q-type VSCC than MVIIA is toward the N-type VSCC. Given the dissimilarities in absolute potency ranges, comparison of the binding results in terms of "relative" potencies reveals that the contribution of Tyr13 in ω-conotoxin VSCC binding may be considered equivalent in the case of N-type and P/Q-type VSCCs (Table 2). However, further comparisons cannot be made as little is known about what residues in MVIIC are important for P/Q-type binding (*47*) and further studies are required to develop SARs for this peptide.

Perhaps one of the intriguing questions raised by this study is why the extensive conformational and orientational changes in loop 2 occur. Using modeling to investigate the effect of an inversion of Tyr13 from the L to D configuration in MVIIC without changing the backbone conformation (unpublished observations) it is apparent that loop 2 requires extensive conformational adjustment to accommodate this change and, in particular, to avoid steric clash between the side chains of Lys10 and Tyr13. An analogous situation is also likely to occur for MVIIA, where disruption to the positioning of Arg10 and Leu11 may be the result of a potential steric clash which would otherwise occur if the backbone conformation were unaltered in [D-Y^{13}]MVIIA.

CONCLUSION

This study supports previous results which show that Tyr13 is important for ω-conotoxin binding to the N-typeVSCC. In addition, the contribution of other residues in loop 2 and the importance of maintaining the structural integrity of this region in terms of conformation and orientation are highlighted. Replacing L- with D-Tyr13 in MVIIA changes the conformation of residues 10−14 without

a significant effect on the β-sheet structural scaffold. This emphasizes the importance of monitoring structure when interpreting changes in the activity of peptides. Configuration inversions are a common technique used to prevent enzyme degradation of peptides, but the ramifications on peptide structure are often overlooked. This study shows that L to D configuration interchanges can have a significant effect on loop structure and not just on the mutated residue. This is especially pertinent to the study of small, biologically active peptides such as the ω-conotoxins.

ACKNOWLEDGMENT

The authors would like to thank Michael Dooley and Alun Jones for advice and Trudy Bond for performing amino acid analyses.

SUPPORTING INFORMATION AVAILABLE

Table of chemical shifts of [D-Y^{13}]MVIIA in aqueous solution. This material is available free of charge via the Internet at http://pubs.acs.org.

REFERENCES

1. Gray, W. R., and Olivera, M. B. (1988) *Annu. Rev. Biochem. 57*, 665−700.
2. Nielsen, K. J., Thomas, L., Lewis, R. J., Alewood, P. F., and Craik., D. J. (1996) *J. Mol. Biol. 263*, 297−310.
3. Myers, R. A., Cruz, L. J., Rivier, J. E., and Olivera, B. M. (1993) *Chem. Rev. 93*, 1923−1936.
4. Valentino, K., Newcomb, R., Gadbois, T., Bowersox, S., Bitner, S., Justice, A., Yamashiro, D., Ciaranello, R., Miljanich, G., and Ramachandran, J. (1993) *Proc. Natl. Acad. Sci. U.S.A. 90*, 7894−7897.
5. Miljanich, G. P. (1997) Venom Peptides as Human Pharmaceuticals. *Sci. Med.* 6−15.
6. Luther, R. R., Tich, N., and Sperzel W. D. (1995) *J. Clin. Pharmacol. 35*, 993−997.
7. McGuire, D., Bowersox, S. S., Fellman, J. D., and Luther R. R. (1997) *J. Cardiovasc. Pharmacol. 35*, 707−734.
8. Haack, J., Kinser, P., Yoshikami, D., and Olivera, B. (1993) *Neuropharmacology 32*, 1151−1159.
9. Lampe, R. A., Lo, M. M. S., Keith, R. A., Horn, B. M., McLane, M. W., Herman, J. L., and Spreen, R. C. (1993) *Biochemistry 32*, 3255−3260.
10. Sato, K., Park, N.-G., Kohno, T., Maeda, T., Kim, J.-I., Kato, R., and Takahashi, M. (1993) *Biochem. Biophys. Res. Commun. 194*, 1292−1296.
11. Kim, J.-I., Takahashi, M., Ogura, A., Kohno, T., Kudo, Y., and Sato, K. (1994) *J. Biol. Chem. 269*, 23876−23878.
12. Kim, J.-I., Takahashi, M., Ohtake, A., Wakamiya, A., and Sato, K. (1995) *Biochem. Biophys. Res. Commun. 206*, 449−454.
13. Miljanich, G. P., Bowersox, S. S., Fox, J. A., Valentino, K. L., Bitner, R. S., and Yamashiro, D. H. (1993) Compositions for delayed treatment of ischemia-related neuronal damage. Publication no. WO 93/10145, International application no. PCT/US92 09766, International Patent Classification, C07K 7/10, A61K 37/02.
14. Nadasdi, L., Yamashiro, D., Chung, D., Tarczyhornoch, K., Adriaenssens, P., and Ramachandran, J. (1995) *Biochemistry 34*, 8076−8081.
15. Lew, M. J., Flinn, J. P., Pallaghy, P. K., Murphy, R., Whorlow, S. L., Wright, C. E., Norton, R. S., and Angus, J. A. (1997) *J. Biol. Chem. 272*, 12014−12023.
16. Wang, Y.-X., Bezprozvannaya, S., Bowersox, S. S., Nadasdi, L., Miljanich, G., Mezo, G., Silva, D., Tarczy-Hornoch, K., and Luther, R. R. (1998) *Naunyn-Schmeideberg's Arch Pharmacol. 357*, 159−168.
17. Shikata, Y., Watanabe, T., Teramoto, T., Inoue, A., Kawakami, Y., Nishizawa, Y., Katayama, K., and Kuwada, M. (1995) *J. Biol. Chem. 270*, 16719−16723.
18. Jimenéz, E. C., Olivera, B. M., Gray, W. R., and Cruz, L. J. (1996) *J. Biol. Chem. 271*, 28002−28005.
19. Bidlingmeyer, B. A., Cohen, S. A., and Tarvin, T. L. (1984) *J. Chromatogr. 336*, 93−104.
20. Schnölzer, M., Alewood, P. F., Jones, A., Alewood D., and Kent, S. B. H. (1992) *Int. J. Pept. Protein Res. 40*, 180−193.
21. Fraker, P. J., and Speck, J. C., Jr. (1978) *Biochem. Biophys. Res. Commun. 80*, 849−857.
22. Ahmed, S. N., and Miljanich, G. P. (1988) *Brain Res. 453*, 247−56.
23. Cruz, L. J., and Olivera, B. M. (1986) *J. Biol. Chem. 261*, 6230−6233.
24. Wagner, J. A., Snowman, A. M., Biswas, A., Olivera, B. M., and Snyder, S. H. (1988) *J. Neurosci. 8* (9), 3354−3359.
25. Kristipati, R., Nadasdi, L, Tarczy-Hornoch, K., Lau, K., Miljanich, G. P., Ramachandran, J., and Bell, J. R. (1994) *Mol. Cell. Neurosci. 5*, 219−228.
26. Rance, M., Sørenson, O. W., Bodenhausen, G., Wagner, G., Ernst, R. R., and Wüthrich, K. (1983) *Biochem. Biophys. Res. Commun. 177*, 479−485.
27. Greisinger, C., Sorenson, O. W., and Ernst, R. R. (1987) *J. Magn. Reson. 75*, 474−492.
28. Jeener, J., Meier, B. H., Bachmann, P., and Ernst, R. R. (1979) *J. Chem. Phys. 71*, 4546−4553.
29. Kumar, A., Ernst, R. R., and Wüthrich, K. (1980) *Biochem. Biophys. Res. Commun.* 95, 1−6.
30. Bax, A., and Davis, D. G. (1985) *J. Magn. Reson. 65*, 355−360.
31. Piotto, M., Saudek, V., and Sklenár, V. (1992) *J. Biolmol. NMR* 2, 661.
32. Wüthrich, K., Billeter, M., and Braun, W. (1983) *J. Mol. Biol. 169*, 949−961.
33. Pardi, A., Billeter, M., and Wüthrich, K. (1984) *J. Mol. Biol. 180*, 741−751.
34. Wagner, G., Braun, W., Havel, T. F., Schaumann, T., Go, N., and Wüthrich, K. (1987) *J. Mol. Biol. 196*, 611−639.
35. Brünger, A. T., Clore, G. M., Gronenborn, A. M., and Karplus, M. (1986) *Proc. Nat. Acad. Sci. U.S.A. 83*, 3801−3805.
36. Brünger, A. T. (1992) X-PLOR version 3.1, A System for X-ray Crystallography and NMR, Yale University, New Haven, CT.
37. Brooks, B., Bruccoli, R., Olafson, B. O., States, D., Swaminathan, S., and Karplus, M. (1983) *J. Comput. Chem. 4*, 187−217.
38. Hyberts, S. G., Goldberg, M. S., Havel, T. S., and Wagner, G. (1992) *Protein Sci. 1*, 736−751.
39. Pallaghy, P. K., Duggan, B. M., Pennington, M. W., and Norton, R. S. (1993) *J. Mol. Biol. 234*, 405−420.
40. Wüthrich, K. (1986) NMR of Proteins, and Nucleic Acids. Wiley-Interscience, New York.
41. Wishart, D. S., Bigam, C. G., Yao, J., Abildgaard, F., Dyason, H. J., Oldfield, E., Markley, J. L., and Sykes, B. D. (1995) *J. Biolmol. NMR 6*, 135−140.
42. Pastore, A., and Saudek, V. (1990) *J. Magn. Reson. 90*, 165−176.
43. Wishart, D. S., Sykes, B. D., and Richards, F. M. (1991) *J. Mol. Biol. 222*, 311−333.
44. Kohno, T., Kim, J. I., Kobayashi, K., Kodera, Y., Maeda, T., and Sato, K. (1995) *Biochemistry 34*, 10256−10265.
45. Basus, V. J., Nadasdi, L., Ramachandran, J., and Miljanich, G. P. (1995) *FEBS Lett. 370*, 163−169.
46. Scanlon, M., Naranjo, D., Thomas, L., Alewood, P. F., Lewis, R. J., and Craik, D. J. (1997) *Structure 5*, 1585−1597.
47. Sato, K., Raymond, C., Martin-Moutot, M., Sasaki, T., Omori, A., Ohtake, A., Kim, J. I., Kohno, T., Takahashi, M., and Seagar, M. (1997) *FEBS Lett. 414*, 480−484.

BI982980U